Laser and Particle Beams (2015), *33*, 201–210.

doi:10.1017/S0263034615000257

Detailed computation of hot-plasma atomic spectra

JEAN-CHRISTOPHE PAIN,[1] FRANCK GILLERON,[1] AND THOMAS BLENSKI[2]
[1]CEA, DAM, DIF, Arpajon, France
[2]CEA, DSM, IRAMIS, Gif-sur-Yvette, France

(Received 6 November 2014; Accepted 9 February 2015)

Abstract

We present recent evolutions of the detailed opacity code SCO-RCG which combines statistical modelings of levels and lines with fine-structure calculations. The code now includes the Partially Resolved Transition Array model, which allows one to replace a complex transition array by a small-scale detailed calculation preserving energy and variance of the genuine transition array and yielding improved higher-order moments. An approximate method for studying the impact of strong magnetic field on opacity and emissivity was also recently implemented. The Zeeman line profile is modeled by fourth-order Gram-Charlier expansion series, which is a Gaussian multiplied by a linear combination of Hermite polynomials. Electron collisional line broadening is often modeled by a Lorentzian function and one has to calculate the convolution of a Lorentzian with Gram-Charlier distribution for a huge number of spectral lines. Since the numerical cost of the direct convolution would be prohibitive, we propose, to obtain the resulting profile, a fast and precise algorithm, relying on a representation of the Gaussian by cubic splines.

Keywords: E1 lines; Fine structure; Hot plasmas; Opacity; Radiative properties; Statistical methods

1. INTRODUCTION

When atomic spectral lines coalesce into broad unresolved patterns due to physical broadening mechanisms (Stark effect, auto-ionization, etc.), they can be handled by the so-called statistical methods (Bauche *et al.*, 1988). Global characteristics – average energy, variance, asymmetry, and sharpness – of level-energy, absorption, or emission spectra can be useful for their analysis and the investigation of their regularities (Bauche & Bauche-Arnoult, 1987; 1990). Systematic studies of these average characteristics for transition arrays and applications to the interpretation of experimental spectra of high-temperature plasmas were initiated in (Moszkowski, 1962; Bauche *et al.*, 1979). The elaboration of the general group-diagrammatic summation method (Ginocchio, 1973) and its realization in computer codes (Kucas & Karazija, 1993; 1995; Kucas *et al.*, 2005; Karazija & Kucas, 2013) opened up new possibilities for the use of global properties in atomic spectroscopy. On the other hand, some transition arrays exhibit a small number of lines that must be taken into account individually. Those lines are important for the plasma diagnostics, interpretation of spectroscopy experiments, and for calculating the Rosseland mean κ_R, important for radiation transport, and defined as

$$\frac{1}{\kappa_R} = \int_0^\infty \frac{1}{\kappa(h\nu)} \frac{\partial B_T(h\nu)}{\partial T} dh\nu \Big/ \int_0^\infty \frac{\partial B_T(h\nu)}{\partial T} dh\nu, \qquad (1)$$

$h\nu$ being the incident photon energy, $\kappa(h\nu)$ the opacity including stimulated emission, T the temperature and $B_T(h\nu)$ Planck's distribution function. The Rosseland mean is very sensitive to the gaps between lines in the spectrum.

These are the reasons why we developed the hybrid opacity code SCO-RCG (Porcherot *et al.*, 2011), which combines statistical methods and fine-structure calculations, assuming local thermodynamic equilibrium. The main features of the code are described in Section 2, the extension to the hybrid approach of the partially resolved transition array (PRTA) model (Iglesias & Sonnad, 2012), which enables one to replace many statistical transition arrays by small-scale detailed line accounting (DLA) calculations, is presented in Section 3 and comparisons with experimental spectra are shown and discussed in Section 4. In Section 5, an approximate modeling of Zeeman effect is proposed together with a fast numerical algorithm for the convolution of a Lorentzian function

Address correspondence and reprint requests to: Jean-Christophe Pain, CEA, DAM, DIF, F-91297 Arpajon, France. E-mail: jean-christophe.pain@cea.fr

with Gram–Charlier expansion series, based on a cubic-spline representation of the Gaussian.

2. DESCRIPTION OF THE CODE AND EFFECT OF DETAILED LINES

In order to decide, for each transition array, whether a detailed treatment of lines is necessary or not and to determine the validity of statistical methods, the SCO-RCG code uses criteria to quantify the porosity (localized absence of lines) of transition arrays. The main quantity involved in the decision process is the ratio between the individual line width and the average energy gap between two neighboring lines in a transition array. Data required for the calculation of lines (Slater, spin-orbit, and dipolar integrals) are provided by SCO code (Blenski *et al.*, 2000), which takes into account plasma screening and density effects on the wave-functions. Then, level energies and lines are calculated by an adapted routine (RCG) of Cowan's atomic-structure code (Cowan, 1981) performing the diagonalization of the Hamiltonian matrix. Transition arrays for which a DLA treatment is not required or impossible are described statistically, by unresolved transition array (UTA; Bauche-Arnoult *et al.*, 1979), spin-orbit split array (SOSA; Bauche-Arnoult *et al.*, 1985) or super transition array (STA; Bar-Shalom *et al.*, 1989) formalisms used in SCO. In SCO-RCG, the orbitals are treated individually up to a certain limit, consistent with Inglis-Teller limit (Inglis & Teller, 1939), beyond which they are gathered in a single super-shell. The grouped orbitals are chosen so that they interact weakly with inner orbitals (this is why we sometimes name that super-shell "Rydberg"). The total opacity is the sum of photo-ionization, inverse Bremsstrahlung, and Thomson scattering spectra calculated by SCO code and a photo-excitation spectrum in the form

$$\kappa(h\nu) = \frac{1}{4\pi\varepsilon_0}\frac{\mathcal{N}}{A}\frac{\pi e^2 h}{mc}\sum_{X\to X'} f_{X\to X'}\mathcal{P}_X\Psi_{X\to X'}(h\nu), \qquad (2)$$

where h is Planck's constant, $\mathcal{N}$ the Avogadro number, ϵ_0 the vacuum polarizability, m the electron mass, A the atomic number, and c the speed of light. $\mathcal{P}$ is a probability, f an oscillator strength, $\Psi(h\nu)$ a profile, and the sum $X\to X'$ runs over lines, UTA, SOSA, or STA of all ion charge states present in the plasma. Special care is taken to calculate appropriately the probability of X (which can be either a level αJ, a configuration C, or a superconfiguration S) because it can be the starting point for different transitions (DLA, UTA, SOSA, STA). In order to ensure the normalization of probabilities, we introduce three disjoint ensembles: $\mathcal{D}$ (detailed levels αJ), $\mathcal{C}$ (configurations C too complex to be detailed), and $\mathcal{S}$ (superconfigurations S that do not reduce to ordinary configurations). The total partition function then reads

$$U_{\rm tot} = U(\mathcal{D}) + U(\mathcal{C}) + U(\mathcal{S}) \quad \text{with} \quad \mathcal{D}\cap\mathcal{C}\cap\mathcal{S} = \varnothing, \qquad (3)$$

where each term is a trace over quantum states of the form $\mathrm{Tr}\left[e^{-\beta(\hat{H}-\mu\hat{N})}\right]$, where $\hat{H}$ is the Hamiltonian, $\hat{N}$ the number operator, μ the chemical potential, and $\beta = 1/(k_{\rm B}T)$. The probabilities of the different species of the N-electron ion are

$$\mathcal{P}_{\alpha J} = \frac{1}{U_{\rm tot}}(2J+1)e^{-\beta(E_{\alpha J}-\mu N)}, \qquad (4)$$

for a level belonging to $\mathcal{D}$,

$$\mathcal{P}_C = \frac{1}{U_{\rm tot}}\sum_{\gamma J\in C}(2J+1)e^{-\beta(E_{\alpha J}-\mu N)}, \qquad (5)$$

for a configuration that can be detailed,

$$\mathcal{P}_C = \frac{1}{U_{\rm tot}}g_C e^{-\beta(E_C-\mu N)} \qquad (6)$$

for a configuration that can not be detailed (i.e., belonging to $\mathcal{C}$) and

$$\mathcal{P}_S = \frac{1}{U_{\rm tot}}\sum_{C\in S} g_C e^{-\beta(E_C-\mu N)} \qquad (7)$$

for a superconfiguration.

We can see in Figure 1 that fine-structure calculations can have a strong impact on the Rosseland mean. The physical broadening mechanisms are the same for both the calculations (statistical: SCO and detailed: SCO-RCG). The modeling of the (impact) collisional broadening relies on the Baranger formulation (Baranger, 1958) and expressions provided by Dimitrijevic and Konjevic (Dimitrijevic & Konjevic, 1987) corrected by inelastic Gaunt factors similar, for high energies, to the ones proposed by Griem *et al.*, (1962; 1968). Ionic Stark effect is treated in the quasi-static

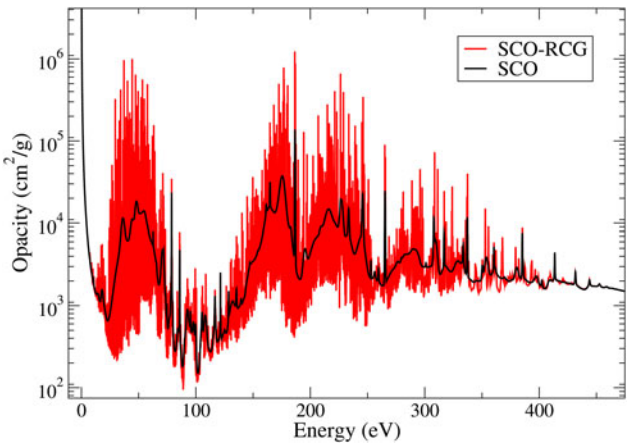

Fig. 1. Comparison between the SCO-RCG and full-statistical (SCO) calculations for an iron plasma at $T = 50$ eV and $\rho = 10^{-3}$ g/cm^2. The Rosseland mean is equal to 1691 cm^2/g for the SCO calculation and to 1261 cm^2/g for SCO-RCG.

https://doi.org/10.1017/S0263034615000257 Published online by Cambridge University Press

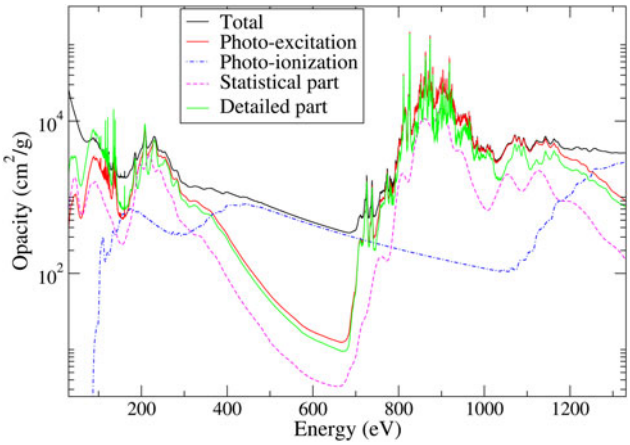

Fig. 2. Different contributions to opacity calculated by SCO-RCG code for an iron plasma at $T = 193$ eV and $\rho = 0.58$ g cm^{-3} (boundary of the convective zone of the Sun). The maximum number of lines potentially detailed per transition array is chosen equal to 100.

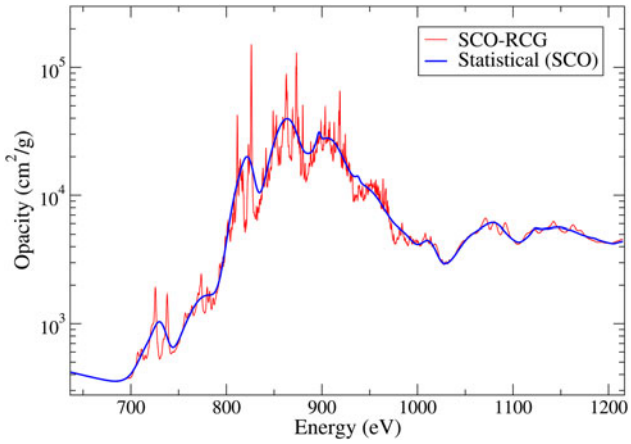

Fig. 4. Comparison between the full-statistical (SCO) spectrum and SCO-RCG around the maximum of the opacity bump in the conditions of Figure 2 (boundary of the convective zone of the Sun). The maximum number of lines potentially detailed per transition array is chosen equal to 800,000.

approximation following an approach proposed by Rozsnyai (1977), corrected in order to reproduce the exact second-order moment of the electric micro-field distribution in the framework of the one-component plasma (OCP) model (Iglesias *et al.*, 1983).

The code can be useful for astrophysical applications (Gilles *et al.*, 2011, Turck-Chieze *et al.*, 2011). Figures 2–4 represent the different contributions to opacity (DLA, statistical, and PRTA) for an iron plasma in conditions corresponding to the boundary of the convective zone of the Sun, with a maximum imposed number N_{max} of detailed lines per transition array equal to 100 and 800,000, respectively. As expected, when N_{max} increases, the statistical part becomes smaller. In Figure 2, the detailed part is obviously not sufficiently larger than the statistical part around $h\nu = 850$ eV.

As shown in Figures 5–7, the statistical calculation (SCO) may depart significantly from the detailed one (SCO-RCG), and the differences are essentially the signature of the porosity of transition arrays. The density being quite low ($\rho = 4 \times 10^3$ g cm^{-3}), the lines emerge clearly in the spectrum. These conditions are accessible to laser spectroscopy experiments (see Section 4) and we can see that the opacity changes notably with temperature. Therefore, even if the quantity which is measured in absorption point-projection-spectroscopy experiments is not the opacity itself, but the transmission (see Section 4), one may expect to have a reliable idea of the plasma temperature during the measurement.

3. ADAPTATION OF THE PRTA MODEL TO THE HYBRID APPROACH

To complement DLA efforts, the code was recently improved (Pain *et al.*, 2013; 2015) with the PRTA model (Iglesias &

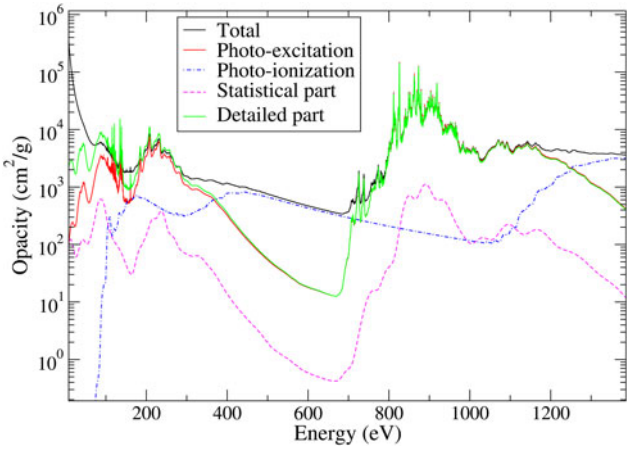

Fig. 3. Different contributions to opacity calculated by SCO-RCG code for an iron plasma at $T = 193$ eV and $\rho = 0.58$ g cm^{-3} (boundary of the convective zone of the Sun). The maximum number of lines potentially detailed per transition array is chosen equal to 800,000.

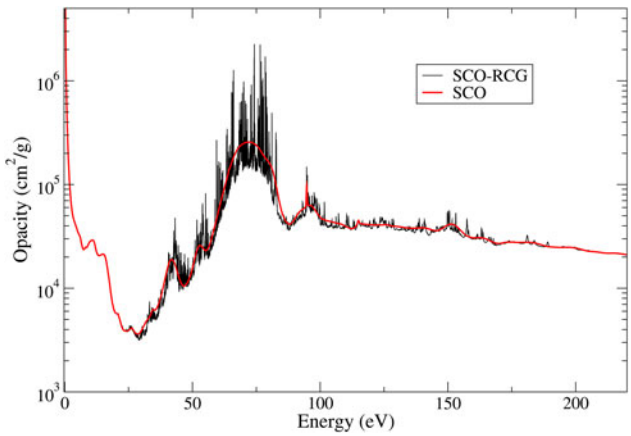

Fig. 5. Iron opacity at $T = 15$ eV and $\rho = 4 \times 10^{-3}$ g cm^{-3}. Comparison between the full-statistical (SCO) and SCO-RCG calculations. The maximum number of lines potentially detailed per transition array is chosen equal to 800,000.

https://doi.org/10.1017/S0263034615000257 Published online by Cambridge University Press

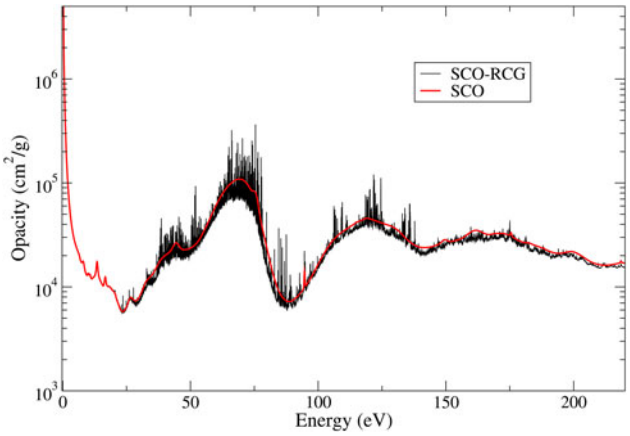

Fig. 6. Iron opacity at $T = 27$ eV and $\rho = 4 \times 10^{-3}$ g cm^{-3}. Comparison between the full-statistical (SCO) and SCO-RCG calculations. The maximum number of lines potentially detailed per transition array is chosen equal to 800,000.

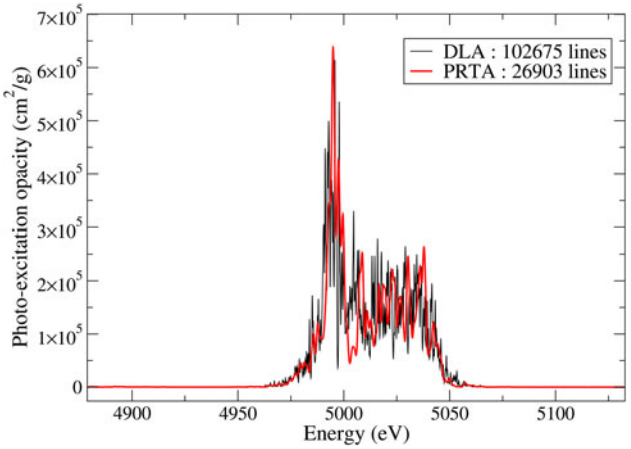

Fig. 8. Comparison between two SCO-RCG calculations relying respectively on DLA and PRTA treatments of lines for transition arrays $3p_{3/2} \rightarrow 5s$ in a Hg plasma at $T = 600$ eV and $\rho = 0.01$ g/cm^3. The DLA calculation contains 102,675 lines and the PRTA 26,903 lines.

Sonnad, 2012), which may replace the single feature of a UTA by a small-scale detailed transition array that conserves the known transition-array properties (energy and variance) and yields improved higher-order moments. In the PRTA approach, open subshells are split into two groups. The main group includes the active electrons and those electrons that couple strongly with the active ones. The other subshells are relegated to the secondary group. A small-scale DLA calculation is performed for the main group (assuming therefore that the subshells in the secondary group are closed) and a statistical approach for the secondary group assigns the missing UTA variance to the lines. In the case where the transition $C \rightarrow C'$ is a UTA that can be replaced by a PRTA (see Fig. 8), its contribution to the opacity is modified according to

$$f_{C\rightarrow C'}\mathcal{P}_C\Psi_{C\rightarrow C'}(h\nu) \approx \sum_{\bar{\alpha}\bar{J}\rightarrow\bar{\alpha}'\bar{J}'} f_{\bar{\alpha}\bar{J}\rightarrow\bar{\alpha}'\bar{J}'}\mathcal{P}_{\bar{\alpha}\bar{J}}\Psi_{\bar{\alpha}\bar{J}\rightarrow\bar{\alpha}'\bar{J}'}(h\nu), \qquad (8)$$

where the sum runs over PRTA lines $\bar{\alpha}\bar{J} \rightarrow \bar{\alpha}'\bar{J}'$ between pseudo-levels of the reduced configurations, $f_{\bar{\alpha}\bar{J}\rightarrow\bar{\alpha}'\bar{J}'}$ is the corresponding oscillator strength and $\Psi_{\bar{\alpha}\bar{J}\rightarrow\bar{\alpha}'\bar{J}'}$ is the line profile augmented with the statistical width due to the other (non-included) spectator subshells. The probability of the pseudo-level $\bar{\alpha}\bar{J}$ of configuration $\bar{C}$ reads

$$\mathcal{P}_{\bar{\alpha}\bar{J}} = \frac{(2\bar{J}+1)e^{-\beta(E_{\bar{\alpha}\bar{J}}-\mu N)}}{\sum_{\bar{\alpha}\bar{J}\in\bar{C}}(2\bar{J}+1)e^{-\beta(E_{\bar{\alpha}\bar{J}}-\mu N)}} \times \mathcal{P}_C \qquad (9)$$

with ensures that $\sum_{\bar{\alpha}\bar{J}\in\bar{C}}\mathcal{P}_{\bar{\alpha}\bar{J}} = \mathcal{P}_C$, where $\mathcal{P}_C$ is the probability of the genuine configuration given in Eq. (4).

Figure 9 represents the different contributions to opacity (DLA, statistical, and PRTA) for an iron plasma in conditions corresponding to the boundary of the convective zone of the Sun. We can see that the PRTA contribution is of the same

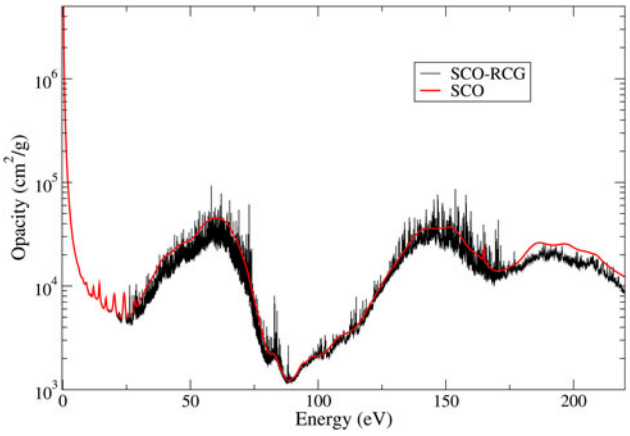

Fig. 7. Iron opacity at $T = 38$ eV and $\rho = 4 \times 10^{-3}$ g cm^{-3}. Comparison between the full-statistical (SCO) and SCO-RCG calculations. The maximum number of lines potentially detailed per transition array is chosen equal to 800,000.

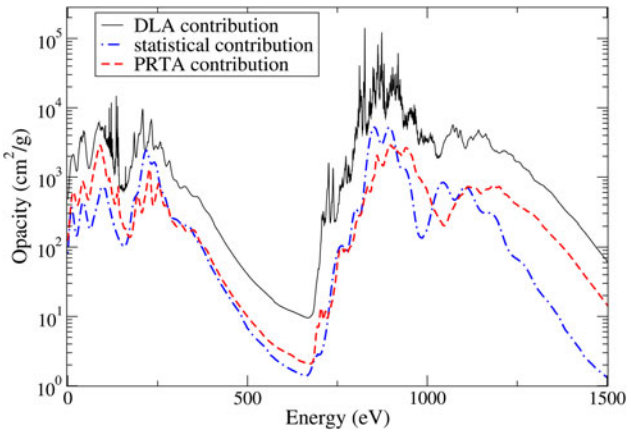

Fig. 9. The three independent contributions to photo-excitation calculated by SCO-RCG code for an iron plasma at $T = 193$ eV and $\rho = 0.58$ g cm^{-3} (boundary of the convective zone of the Sun).

https://doi.org/10.1017/S0263034615000257 Published online by Cambridge University Press

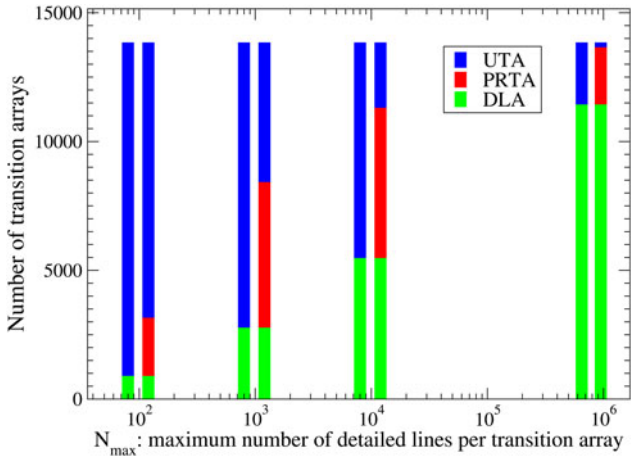

Fig. 10. Number of DLA, PRTA, and UTA for different values of the maximum number of detailed lines imposed: 10^2, 10^3, 10^4, and 10^6. For each case, two histograms are displayed: In the first one, the detailed calculations are only pure DLA and in the second one they can be either DLA or PRTA.

order of magnitude here as the statistical one. The calculation was performed with a maximum imposed of 10,000 detailed lines per transition arrays. We can see in Figure 10 that for each value of the maximum number of lines that can be detailed ($N_{\max}$), some UTA are replaced by PRTA transition arrays. Of course, the number of remaining UTA decreases with $N_{\max}$.

4. INTERPRETATION OF EXPERIMENTAL SPECTRA

The SCO-RCG code has been successfully compared with several absorption and emission experimental spectra, measured in experiments at several laser (Fig. 11) or *Z*-pinch facilities (Fig. 12). The comparisons show the relevance of

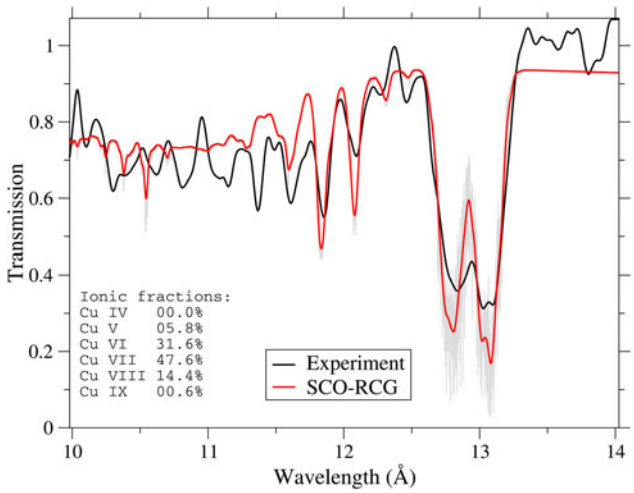

Fig. 11. Interpretation with SCO-RCG code of the copper spectrum ($2p\rightarrow3d$ transitions) measured by Loisel et al. (Loisel et al., 2009; Blenski et al., 2011*a*; 2011*b*). The temperature is $T = 16$ eV and the density $\rho = 5\times10^{-3}$ g cm^3.

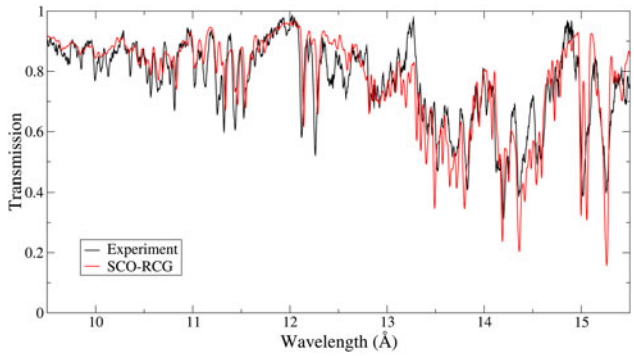

Fig. 12. Interpretation with SCO-RCG code of the iron spectrum ($2p\rightarrow3d$ transitions) measured by Bailey et al. (2007). The temperature is $T =$ 150 eV and the density $\rho = 0.058$ g cm^3.

the hybrid model and the necessity to carry out detailed calculations instead of full statistical calculations. As mentioned in Section 2, the quantity which is measured experimentally is the transmission, related to the opacity by Beer–Lambert–Bouguer's law:

$$T(h\nu) = e^{-\rho L\kappa(h\nu)}, \tag{10}$$

where L is the thickness of the sample. The relation (10) between transmission and opacity is valid under the assumption that the material is optically thin and that re-absorption processes are neglected.

In SCO-RCG, configuration interaction is limited to electrostatic one between relativistic sub-configurations ($n\ell j$ orbitals) belonging to a non-relativistic configuration ($n\ell$ orbitals), namely "relativistic configuration interaction". That effect has a strong impact on the ratio of the two relativistic substructures of the $2p\rightarrow3d$ transition on Figure 11.

5. STATISTICAL MODELING OF ZEEMAN EFFECT

5.1. Determination of the Moments

Quantifying the impact of a magnetic field on spectral line shapes is important in astrophysics, in inertial confinement fusion (ICF) or for *Z*-pinch experiments. Because the line computation becomes even more tedious in that case, we propose, to avoid the diagonalization of the Zeeman Hamiltonian, to describe Zeeman patterns in a statistical way. This is also justified by the fact that in a hot plasma, the number of lines is huge, and therefore the number of Zeeman transitions, arising from the splitting of spectral lines, is even greater, which makes the coalescence of the spectral features more important. Due to the other physical broadening mechanisms, the Zeeman components can not be resolved (Doron *et al.*, 2014).

In the presence of a magnetic field B, a level αJ_1 (energy E_1) splits into $2J_1 + 1$ states M_1 ($-J_1 \le M_1 \le J_1$) of energy $E_1+\mu_B g_1 M_1$, μ_B being the Bohr magneton and g_1 the Landé factor in intermediate coupling (provided by RCG

https://doi.org/10.1017/S0263034615000257 Published online by Cambridge University Press

routine). Each line splits into three components associated with the selection rule $\Delta M = q$, where $q = 0$ for a π component and ± 1 for a $\sigma_\pm$ component. The intensity of a component can be characterized by the strength-weighted moments of the energy distribution. The nth-order moment reads

$$\mu_n[q] = 3 \sum_{M_1,M_2} \begin{pmatrix} J_1 & 1 & J_2 \\ -M_1 & -q & M_2 \end{pmatrix}^2 \times (E_2 - E_1 + \mu_B B[g_2 M_2 - g_1 M_1])^n , \quad (11)$$

which can be evaluated analytically (Pain & Gilleron, 2012*a*; 2012*b*), using graphical representation of Racah algebra or Bernoulli polynomials (Mathys & Stenflo, 1987).

5.2. Gram–Charlier Distribution

Gram–Charlier expansions are useful to model densities which are deviations from the normal one. The expansion is named after the Danish mathematician Jorgen P. Gram (1850–1916) and the Swedish astronomer Carl V. L. Charlier (1862–1934). Historical accounts of the origin of the Gram–Charlier expansion are given in Hald (2000) and Davis (2005). This expansion, that finds applications in many areas, including finance (Jondeau & Rockinger, 2001), analytical chemistry (Di Marco & Bombi, 2001), spectroscopy (O'Brien, 1992), and astrophysics and cosmology (Blinnikov & Moessner, 1998) reads

$$GC(u) = \frac{1}{\sqrt{2\pi v}} e^{-u^2/2} \left[\sum_{k=0}^{\infty} c_k \mathrm{He}_k\left(\frac{u}{\sqrt{2}}\right) 2^{-k/2} \right], \quad (12)$$

where $u = (h\nu - \mu_1)/\sqrt{v}$, $v = \mu_2 - (\mu_1)^2$ being the variance. The polynomials $\mathrm{He}_k(x)$ can be expressed as

$$\mathrm{He}_k(x) = \frac{1}{2^{k/2}} \mathrm{H}_k\left(\frac{x}{\sqrt{2}}\right), \quad (13)$$

where $\mathrm{H}_k(x)$ are the usual Hermite polynomials obeying the recurrence relation (Szego, 1939):

$$\mathrm{H}_{k+1}(x) = 2x\mathrm{H}_k(x) - 2k\mathrm{H}_{k-1}(x) \quad (14)$$

initialized with $H_0(x) = 1$ and $H_1(x) = 2x$. The coefficients c_k are given by

$$c_k = \sum_{j=0}^{[k/2]} \frac{(-1)^j}{j!(k-2j)!2^j} \alpha_{k-2j} \quad (15)$$

where [.] denotes the integer part and α_k is the dimensionless centered k-order moment of the distribution

$$\alpha_k = \left(\sum_{p=0}^{k} \begin{pmatrix} k \\ p \end{pmatrix} \mu_p (-\mu_1)^{k-p} \right) / v^{k/2}. \quad (16)$$

Table 1. *Values of α_3 and α_4 of the Zeeman components.* $J_< = min(J_1,J_2)$ *and* $J_> = min(J_1,J_2)$. *sgn[x] is the sign of* x.

		$J_2 = J_1$	$J_2 = J_1 \pm 1$
σ_q	α_3	$(-1)^q q(J_1 - J_2)\mathrm{sgn}[g_1 - g_2]\frac{2\sqrt{5}}{3\sqrt{3}}\frac{J_>}{\sqrt{J_<(J_>+1)}}$	
	α_4	$\frac{5}{7}\left(\frac{12J_1(J_1+1)-17}{4J_1(J_1+1)-3}\right)$	$\frac{5}{21}\left(13 - \frac{4}{J_<(J_>+1)}\right)$
π	α_3	0	
	α_4	$\frac{25}{7}\left(\frac{3[(J_1+2)J_1^2-1]J_1+1}{[1-3J_1(J_1+1)]^2}\right)$	$\frac{5}{7}\left(3 - \frac{2}{J_<(J_>+1)}\right)$

A good representation of the Zeeman profile is obtained using, for each component, the fourth-order Gram–Charlier expansion series:

$$\Psi_Z(u) = \frac{1}{\sqrt{2\pi v}} \exp\left(-\frac{u^2}{2}\right) \left[1 - \frac{\alpha_3}{2}\left(u - \frac{u^3}{3}\right) + \frac{(\alpha_4 - 3)}{24}\left(3 - 6u^2 + u^4\right) \right], \quad (17)$$

where α_3 (skewness) and α_4 (kurtosis) quantify respectively the asymmetry and the sharpness of the component (see Table 1) (Kendall & Stuart, 1969). This approximate method was shown to provide quite a good description (see Fig. 13) of the effect of a strong magnetic field on spectral lines (Pain & Gilleron, 2012*a*; 2012*b*). The contribution of a magnetic field to an UTA can be taken into account roughly by adding a contribution $2/3(\mu_B B)^2 \approx 3.35 \times 10^{-5}$ $[B(MG)]^2$ eV^2 to the statistical variance.

When all the other broadening mechanisms (statistical, Doppler, and ionic Stark) are described by a Gaussian, the resulting profile (convolution of a Gaussian by Gram–Charlier) remains a Gram–Charlier function with modified moments. However, electron collisional broadening is usually modeled

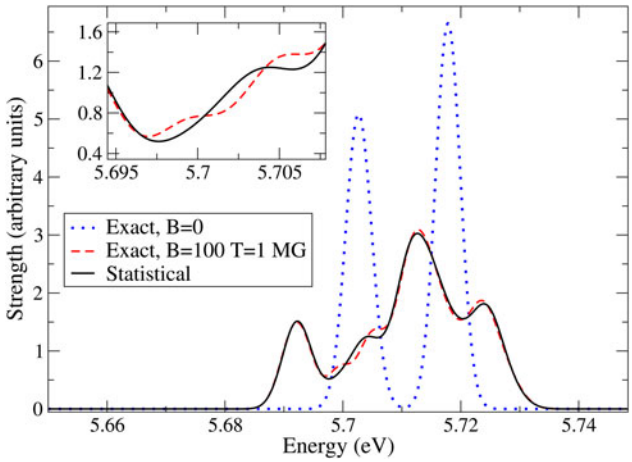

Fig. 13. Effect of a 1 MG magnetic field on triplet transition $1s2s\ ^3S \rightarrow 1s2p\ ^3P$ of carbon ion C^{4+} with a convolution width (full width at half maximum) of 0.005 eV. The observation angle θ is such that $\cos^2(\theta) = 1/3$.

https://doi.org/10.1017/S0263034615000257 Published online by Cambridge University Press

by a Lorentzian function

$$L(h\nu, a) = \frac{a}{\pi}\frac{1}{a^2 + (h\nu)^2}, \tag{18}$$

as well as natural width. The convolution of a Gaussian by a Lorentzian leads to a Voigt profile (Voigt, 1912; Matveev, 1972; 1981; Ida *et al.*, 2000) but in the presence of a magnetic field, the problem is more complicated, since the numerical cost of the direct numerical convolution of a Lorentzian with Gram–Charlier function is prohibitive, due to the huge number of lines involved in the computation. It reads

$$C(t) = (GC \otimes L)(t) = \int_{-\infty}^{\infty} GC(u)L(t-u, \lambda)du, \tag{19}$$

where $t = h\nu/\sigma$, $\sigma = \sqrt{v}$ being the standard deviation of the distribution and $\lambda = a/\sigma$.

5.3. Convolution of a Lorentzian function with Gram–Charlier Expansion Series

The convolution product (19) requires the evaluation of a cumbersome integral which reads

$$C(t) = \frac{1}{\pi\sqrt{2\pi}}\frac{\lambda}{\sigma}\int_{-\infty}^{\infty}\frac{e^{-u^2/2}}{\lambda^2 + (t-u)^2} \times \left[\sum_{k=0}^{\infty} c_k \mathrm{He}_k\left(\frac{u}{\sqrt{2}}\right)2^{-k/2}\right]du. \tag{20}$$

In order to fasten the calculation, the Gaussian is sampled at the points $u = -m, -m+1, \ldots, 0, \ldots, m-1, m$ (in practice we use $m = 6$) and interpolated using cubic splines (de Boor, 1978) on each interval $[k,k+1]$ by the formula

$$e^{-u^2/2} = a_k + b_k u + c_k u^2 + d_k u^3. \tag{21}$$

The coefficients a_k, b_k, c_k, and d_k in the interval $[k,k+1]$ are determined by the continuity of the function and its derivative at the points $u = k$ and $u = k+1$. The resulting expressions are given in Table 2. The Gaussian is assumed to be zero for $|u| > m$. Limiting Gram–Charlier expansion series to fourth order [see Eq. (17)], one now has to deal with the convolution of a Lorentzian by a polynomial of order 7. This can be written[1]

$$C(t) = \frac{1}{\pi\sqrt{2\pi}\sigma}\sum_{p=-m}^{m-1}\sum_{k=0}^{7}\gamma_{p,k}S_{p,k}(t), \tag{22}$$

where the coefficients $\gamma_{p,k}$ of the polynomial are given in

[1] In the general case, the upper bound of the sum over k is equal to $N+3$, where N is the order of the Gram-Charlier expansion series.

Table 2. *Expression of the coefficients* a_k, b_k, c_k, *and* d_k *involved in the cubic-spline representation of the Gaussian [Eq. (21)] for* $k \le u \le k+1$

a_k	$e^{-(k+1)^2/2}[k^2(k+2)^2 + e^{k+1/2}(k^2-1)^2]$
b_k	$e^{-(k+1)^2/2}k(k+1)[8+3k+e^{k+1/2}(3k-5)]$
c_k	$e^{-(k+1)^2/2}[4+10k+3k^2+e^{k+1/2}(3k^2-4k-3)]$
d_k	$-e^{-(k+1)^2/2}[3+e^{k+1/2}(k-2)+k]$

Table 3, and

$$S_{p,k}(t) = \int_p^{p+1}\frac{u^k}{\lambda^2+(t-u)^2}du = \frac{1}{\lambda}\sum_{\ell=0}^{k}\binom{k}{\ell}\lambda^\ell t^{k-\ell}\left[\phi_\ell\left(\frac{p+1-t}{\lambda}\right) - \phi_\ell\left(\frac{p-t}{\lambda}\right)\right]. \tag{23}$$

The function $\phi_\ell(w)$ is equal to

$$\phi_\ell(w) = \frac{w^{\ell+1}}{\ell+1}{}_2F_1\left(\begin{matrix}1, \frac{\ell+1}{2} \\ \frac{\ell+3}{2}\end{matrix}; -w^2\right), \tag{24}$$

where ${}_2F_1$ is a hypergeometric function, but can be efficiently obtained using the recurrence relation

$$\phi_\ell(w) = w^{\ell-2} - \phi_{\ell-2}(w) \tag{25}$$

with

$$\phi_0(w) = \arctan(w) \quad \text{and} \quad \phi_1(w) = \frac{1}{2}\ln[1+w^2]. \tag{26}$$

Such a method provides fast and accurate results, even for very asymmetrical and sharp Gram–Charlier distribution (see Fig. 14). The total line profile results from the convolution of Ψ_Z with other broadening mechanisms. If $\sigma \le a/10$, we take only the Lorentzian $L(h\nu,a)$. On the other hand, if $a \le \sigma/150$, we keep the Gaussian. If one has to convolve $C(t)$ by an additional Gaussian of variance σ' (representing Doppler broadening for instance), σ, α_3, and α_4 must be replaced,

$$\begin{cases} \tilde{\sigma} = \sqrt{\sigma^2 + \sigma'^2} \\ \tilde{\alpha}_3 = \alpha_3\left(\dfrac{\tilde{\sigma}}{\sigma}\right)^3 \\ \tilde{\alpha}_4 = \alpha_4\left(\dfrac{\tilde{\sigma}}{\sigma}\right)^4 \end{cases} \tag{27}$$

Figures 15 and 16 illustrate the impact of a 10 MG magnetic field (typical of ICF) in the XUV range for a carbon plasma at $T = 50$ eV and $\rho = 0.01$ g/cm^3.

https://doi.org/10.1017/S0263034615000257 Published online by Cambridge University Press

Table 3. *Coefficients* $\gamma_{\mathrm{p,i}}$ *involved in Eq. (22).*

i	$\gamma_{p,i}$
0	$\left[1+\frac{\alpha_4-3}{8}\right]\boldsymbol{a}_p$
1	$-\frac{\alpha_3}{2}\boldsymbol{a}_p+\left[1+\frac{(\alpha_4-3)}{8}\right]\boldsymbol{b}_p$
2	$-\frac{(\alpha_4-3)}{4}\boldsymbol{a}_p-\frac{\alpha_3}{2}\boldsymbol{b}_p+\left[1+\frac{(\alpha_4-3)}{8}\right]\boldsymbol{c}_p$
3	$\frac{\alpha_3}{6}\boldsymbol{a}_p-\frac{(\alpha_4-3)}{4}\boldsymbol{b}_p-\frac{\alpha_3}{2}\boldsymbol{c}_p+\left[1+\frac{(\alpha_4-3)}{8}\right]\boldsymbol{d}_p$
4	$\frac{(\alpha_4-3)}{24}\boldsymbol{a}_p+\frac{\alpha_3}{6}\boldsymbol{b}_p-\frac{(\alpha_4-3)}{4}\boldsymbol{c}_p-\frac{\alpha_3}{2}\boldsymbol{d}_p$
5	$\frac{(\alpha_4-3)}{24}\boldsymbol{b}_p+\frac{\alpha_3}{6}\boldsymbol{c}_p-\frac{(\alpha_4-3)}{4}\boldsymbol{d}_p$
6	$\frac{(\alpha_4-3)}{24}\boldsymbol{c}_p+\frac{\alpha_3}{6}\boldsymbol{d}_p$
7	$\frac{(\alpha_4-3)}{24}\boldsymbol{d}_p$

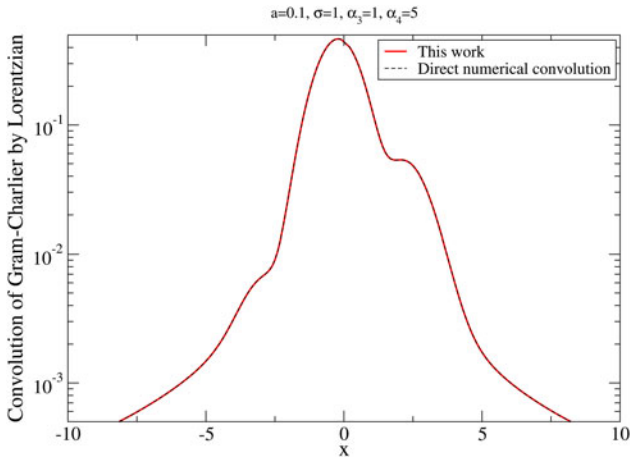

Fig. 14. Convolution of Gram-Charlier expansion series with a Lorentzian. The parameters are $a = 0.1$, $\sigma = 1$, $\alpha_3 = 1$, and $\alpha_4 = 5$. The present approach (red curve) relying on a cubic-spline representation of the Gaussian and the direct numerical convolution (dashed black curve) are superimposed.

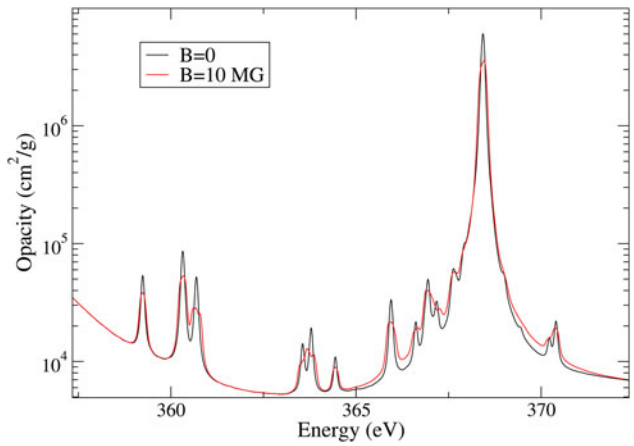

Fig. 15. SCO-RCG calculations (transitions $1s \rightarrow 2p$) with and without magnetic field for a carbon plasma at $T = 50$ eV and $\rho = 10^{-2}$ g cm^{-3} (conditions typical to ICF).

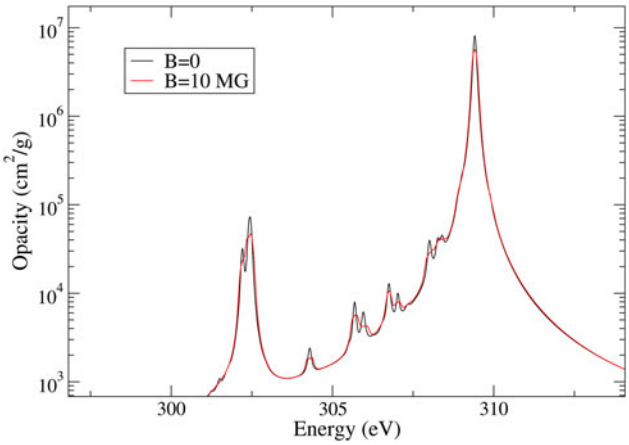

Fig. 16. SCO-RCG calculations (transitions $1s \rightarrow 2p$) with and without magnetic field for a carbon plasma at $T = 50$ eV and $\rho = 10^{-2}$ g cm^{-3} (conditions typical to ICF) in a spectral range close to the one of Figure 15.

6. CONCLUSION

By combining different degrees of approximation of the atomic structure (levels, configurations, and superconfigurations), the SCO-RCG code allows us to explore a wide range of applications, such as the calculation of Rosseland means, the generation of opacity tables, or the spectroscopic interpretation of high-resolution spectra. The PRTA model was recently adapted to the hybrid statistical/detailed approach in order to reduce the statistical part and speed up the calculations. An approximate approach providing a fast and quite accurate estimate of the effect of an intense magnetic field on opacity was also implemented. The formalism requires the moments of the Zeeman components of a line $\alpha J \rightarrow \alpha' J'$, which can be obtained analytically in terms of the quantum numbers and Landé factors and the profile is modeled by the fourth-order A-type Gram–Charlier expansion series. We also proposed a fast and accurate method to perform the convolution of this Gram–Charlier series with a Lorentzian function. Such an algorithm is useful in order to account for distorsions of the Voigt profile, since the direct numerical evaluation of the integral becomes rapidly prohibitive. More generally, it can be helpful for models relying on the theory of moments (Bancewicz & Karwowski, 1987), used in most opacity and emissivity codes. In the future, we plan to extend the statistical modeling of Zeeman effect using temperature-dependent moments (see Appendix) and to improve the treatment of Stark broadening in order to increase the capability of the code as concerns *K*-shell spectroscopy.

Appendix A: Temperature-Dependent Moments of Zeeman Hamiltonian

Polarized synchrotron radiation can be used to determine the magnitude, the orientation and the temperature and magnetic-field dependence of the local rare-earth magnetic moment in magnetically ordered materials. Thole *et al.*

https://doi.org/10.1017/S0263034615000257 Published online by Cambridge University Press

(1985) proposed a theory which predicts an anomalously large magnetic dichroïsm in the $M_{4,5}$ X-ray absorption-edge structure. The square of the matrix element of an optical dipole transition from a state αJM to a final state $\alpha' J' M'$ is, according to the Wigner–Eckart theorem, proportional to the square of the 3*j* symbol times the reduced matrix element (line strength in the absence of a magnetic field):

$$S_{\alpha JM,\alpha' J' M'} = \begin{pmatrix} J & 1 & J' \\ M & q & -M' \end{pmatrix}^2 |\langle \alpha J||C^{(1)}||\alpha' J'\rangle|^2, \quad (28)$$

where α labels different levels of equal J and $q = 0$ for light polarized in the field direction, $q = \pm 1$ for right- or left-circularly polarized light perpendicular to the field direction. The partition function associated to a particular level αJ reads

$$Z_{\alpha J} = \sum_{M=-J}^{J} e^{-C_{\alpha J} M} = \frac{\sinh[C_{\alpha J}(J+1/2)]}{\sinh(C_{\alpha J}/2)}, \quad (29)$$

where $C_{\alpha J} = \mu_B B g_{\alpha J}/(k_B T)$, μ_B being the Bohr magneton, B the intensity of the magnetic field, and $g_{\alpha J}$ the Landé factor of level αJ in intermediate coupling. The first-order moment can be expressed as

$$\begin{aligned} \langle M\rangle &= \frac{1}{Z_{\alpha J}} \sum_{M=-J}^{J} M e^{-C_{\alpha J} M} = -(J+1/2) \\ &\quad \times \coth[C_{\alpha J}(J+1/2)] + \frac{1}{2}\coth(C_{\alpha J}/2) \\ &= -JB_J(C_{\alpha J} J), \end{aligned} \quad (30)$$

where B_J denotes Brillouin's function (Darby, 1967; Subramanian, 1986):

$$B_J(x) = \frac{2J+1}{2J}\coth\left(\frac{2J+1}{2J}x\right) - \frac{1}{2J}\coth\left(\frac{x}{2J}\right). \quad (31)$$

For $<M^2>$, one has

$$\langle M^2\rangle = \frac{1}{Z_{\alpha J}} \sum_{M=-J}^{J} M^2 e^{-C_{\alpha J} M} = J(J+1) + \langle M\rangle \coth(C_{\alpha J}/2) \quad (32)$$

and the higher-order moments can be obtained using the following relation:

$$\langle M^n\rangle = \frac{(-1)^n}{Z_{\alpha J}} \frac{\partial^n Z_{\alpha J}}{\partial C_{\alpha J}^n} = \langle M\rangle\langle M^{n-1}\rangle - \frac{\partial}{\partial C_{\alpha J}}\langle M^{n-1}\rangle, \quad (33)$$

where $n \in N$.

ACKNOWLEDGMENT

The authors have presented their paper in Proceedings of the 33rd ECLIM (European Conference on Laser Interaction with Matter), 30th August– 5th September 2014, Paris, France.

REFERENCES

Bailey, J.E., Rochau, G.A., Iglesias, C.A., Abdallah Jr., J., Macfarlane, J.J., Golovkin, I., Wang, P., Mancini, R.C., Lake, P.W., Moore, T.C., Bump, M., Garcia, O. & Mazevet, S. (2007). Iron-plasma transmission measurements at temperatures above 150 eV. *Phys. Rev. Lett.* **99**, 265002.

Bancewicz, M. & Karwowski, J. (1987). On moment-generated spectra of atoms. *Physica* **145C**, 241–248.

Baranger, M. (1958). Problem of overlapping lines in the theory of pressure broadening. *Phys. Rev.* **111**, 494–504.

Bar-Shalom, A., Oreg, J., Goldstein, W.H., Shvarts, D. & Zigler, A. (1989). Super-transition-arrays: A model for the spectral analysis of hot, dense plasmas. *Phys. Rev. A* **40**, 3183–3193.

Bauche-Arnoult, C., Bauche, J. & Klapisch, M. (1979). Variance of the distributions of energy levels and of the transition arrays in atomic spectra. *Phys. Rev. A* **20**, 2424–2439.

Bauche-Arnoult, C., Bauche, J. & Klapisch, M. (1985). Variance of the distributions of energy levels and of the transition arrays in atomic spectra. III. Case of spin-orbit-split arrays. *Phys. Rev. A* **31**, 2248–2259.

Bauche, J. & Bauche-Arnoult, C. (1987). Level and line statistics in atomic spectra. *J. Phys. B: At. Mol. Opt. Phys.* **20**, 1659–1677.

Bauche, J. & Bauche-Arnoult, C. (1990). Statistical properties of atomic spectra. *Comput. Phys. Rep.* **12**, 3–28.

Bauche, J., Bauche-Arnoult, C. & Klapisch, M. (1988). Transition arrays in the spectra of ionized atoms. *Adv. At. Mol. Opt. Phys.* **23**, 131–195.

Blenski, T., Grimaldi, A. & Perrot, F. (2000). A superconfiguration code based on the local density approximation. *J. Quant. Spectrosc. Radiat. Transfer* **65**, 91–100.

Blenski, T., Loisel, G., Poirier, M., Thais, F., Arnault, P., Caillaud, T., Fariaut, J., Gilleron, F., Pain, J.-C., Porcherot, Q., Reverdin, C., Silvert, V., Villette, B., Bastiani-Ceccotti, S., Turck-Chieze, S., Foelsner, W. & De Gaufridy De Dortan, F. (2011*a*). Opacity of iron, nickel and copper plasmas in the X-ray wavelength range: Theoretical interpretation of the 2p-3d absorption spectra measured at the LULI2000 facility. *Phys. Rev. E* **84**, 036407.

Blenski, T., Loisel, G., Poirier, M., Thais, F., Arnault, P., Caillaud, T., Fariaut, J., Gilleron, F., Pain, J.-C., Porcherot, Q., Reverdin, C., Silvert, V., Villette, B., Bastiani-Ceccotti, S., Turck-Chieze, S., Foelsner, W. & De Gaufridy De Dortan, F. (2011*b*). Theoretical interpretation of X-rays photo-absorption in medium-Z elements plasmas measured at LULI2000 facility. *High Energy Density Phys.* **7**, 320–326.

Blinnikov, S. & Moessner, R. (1998). Expansions for nearly Gaussian distributions. *Astron. Astrophys. Suppl. Ser.* **130**, 193–205.

Cowan, R.D. (1981). *The Theory of Atomic Structure and Spectra*. Berkeley: University of California.

Darby, M.I. (1967). Tables of the Brillouin function and of the related function for the spontaneous magnetization. *Br. J. Appl. Phys.* **18**, 1415–1417.

Davis, A.W. (2005). Gram–Charlier series. In *Encyclopedia of Statistical Sciences*. 2nd edn., Vol. 3. New York: Wiley-Interscience.

De Boor, C. (1978). *A Practical Guide to Splines Series: Applied Mathematical Sciences*, 27. New York: Springer-Verlag.

Di Marco, V.B. & Bombi, G.G. (2001). Mathematical functions for the representation of chromatographic peaks. *J. Chromatogr. A* **931**, 1–30.

https://doi.org/10.1017/S0263034615000257 Published online by Cambridge University Press

Dimitrijevic, M.S. & Konjevic, N. (1987). Simple estimates for Stark broadening of ion lines in stellar plasmas. *Astron. Astrophys.* **172**, 345–349.

Doron, R., Mikitchuk, D., Stollberg, C., Rosenzweig, G., Stambulchik, E., Kroupp, E., Maron, Y. & Hammer, D.A. (2014). Determination of magnetic fields based on the Zeeman effect in regimes inaccessible by Zeeman-splitting spectroscopy. *High Energy Density Phys.* **10**, 56–60.

Gilles, D., Turck-Chieze, S., Loisel, G., Piau, L., Ducret, J.-E., Poirier, M., Blenski, T., Thais, F., Blancard, C., Cosse, P., Faussurier, G., Gilleron, F., Pain, J.-C., Porcherot, Q., Guzik, J.A., Kilcrease, D.P., Magee, N.H., Harris, J., Busquet, M., Delahaye, F., Zeippen, C.J. & Bastiani-Ceccotti, S. (2011). *Comparison of Fe and Ni opacity calculations for a better understanding of pulsating stellar envelopes. High Energy Density Phys.* **7**, 312–319.

Ginocchio, J.N. (1973). Operator averages in a shell-model basis. *Phys. Rev. C* **8**, 135–145.

Griem, H.R. (1968). Semi-empirical formulas for the electron-impact widths and shifts of isolated ion lines in a plasma. *Phys. Rev.* **165**, 258–266.

Griem, H.R., Baranger, M., Kolb, A.C. & Oertel, G.K. (1962). Stark broadening of neutral helium lines in a plasma. *Phys. Rev.* **125**, 177–195.

Hald, A. (2000). The early history of the cumulants and the Gram–Charlier series. *Int. Stat. Rev.* **68**, 137–153.

Ida, T., Ando, M. & Toraya, H. (2000). Extended pseudo-Voigt function for approximating the Voigt profile. *J. Appl. Crystallogr.* **33**, 1311–1316.

Iglesias, C.A., Lebowitz, J.L. & Macgowan, D. (1983). Electric microfield distributions in strongly coupled plasmas. *Phys. Rev. A* **28**, 1667–1672.

Iglesias, C.A. & Sonnad, V. (2012). Partially resolved transition array model for atomic spectra. *High Energy Density Phys.* **8**, 154–160.

Inglis, D.R. & Teller, E. (1939). Ionic depression of series limits in one-electron spectra. *Astrophys. J.* **A90**, 439–448.

Jondeau, E. & Rockinger, M. (2001). Gram–Charlier densities. *J. Econ. Dyn. Control* **25**, 1457–1483.

Karazija, R. & Kucas, S. (2013). Average characteristics of the configuration interaction in atoms and their applications. *J. Quant. Spectrosc. Radiat. Transfer* **129**, 131–144.

Kendall, M.G. & Stuart, A. (1969). *The Advanced Theory of Statistics*, 3rd edn. London: Griffin.

Kucas, S., Jonauskas, V. & Karazija, R. (2005). Calculation of HCI spectra using their global characteristics. *Nucl. Instrum. Methods Phys. Res. B* **235**, 155–159.

Kucas, S. & Karazija, R. (1993). Global characteristics of atomic spectra and their use for the analysis of spectra. I. energy level spectra. *Phys. Scr.* **47**, 754–764.

Kucas, S. & Karazija, R. (1995). Global characteristics of atomic spectra and their use for the analysis of spectra. II. characteristic emission spectra. *Phys. Scr.* **51**, 566–577.

Loisel, G., Arnault, P., Bastiani-Ceccotti, S., Blenski, T., Caillaud, T., Fariaut, J., Foelsner, W., Gilleron, F., Pain, J.-C., Poirier, M., Reverdin, C., Silvert, V., Thais, F., Turck-Chieze, S. & Villette, B. (2009). Absorption spectroscopy of mid and neighboring Z plasmas: Iron, nickel, copper and germanium. *High Energy Density Phys.* **5**, 173–181.

Mathys, G. & Stenflo, J.O. (1987). Anomalous Zeeman effect and its influence on the line absorption and dispersion coefficients. *Astron. Astrophys.* **171**, 368–377.

Matveev, V.S. (1972). Approximate representation of absorption coefficient and equivalent widths of lines with Voigt profile. *Zhurnal Prikladnoi Spectroskopii* **16**, 228–233.

Matveev, V.S. (1981). Approximate representations of the refractive index of a medium in the region of a Voigt-profile absorption line. *Zhurnal Prikladnoi Spectroskopii* **35**, 528–532.

Moszkowski, S.A. (1962). On the energy distribution of terms and line arrays in atomic spectra. *Progr. Theor. Phys.* **28**, 1–23.

O'brien, M.C.M. (1992). Using the Gram–Charlier expansion to produce vibronic band shapes in strong coupling. *J. Phys.: Condens. Matter* **4**, 2347–2359.

Pain, J.-C. & Gilleron, F. (2012*a*). Description of anomalous Zeeman patterns in stellar astrophysics. *EAS Publications Series* **58**, 43–50.

Pain, J.-C. & Gilleron, F. (2012*b*). Characterization of anomalous Zeeman patterns in complex atomic spectra. *Phys. Rev. A* **85**, 033409.

Pain, J.-C., Gilleron, F., Porcherot, Q. & Blenski, T. (2013). The hybrid opacity code SCO-RCG: Recent developments. Proc. of the 40th EPS Conf. on Plasma Physics, P4.403 (2013). http://ocs.ciemat.es/EPS2013PAP/pdf/P4.403.pdf.

Pain, J.-C., Gilleron, F., Porcherot, Q. & Blenski, T. (2015). The Hybrid Detailed/Statistical opacity code SCO-RCG: New developments and applications. Proc. of the 18th Conf. on Atomic Physics in Plasmas. *AIP Conf. Proc.*, in press.

Porcherot, Q., Pain, J.-C., Gilleron, F. & Blenski, T. (2011). A consistent approach for mixed detailed and statistical calculation of opacities in hot plasmas. *High Energy Density Phys.* **7**, 234–239.

Rozsnyai, B.F. (1977). Spectral lines in hot dense matter. *J. Quant. Spectrosc. Radiat. Transfer* **17**, 77–88.

Subramanian, P.R. (1986). Evaluation of $Tr(J_\chi^{2p})$ using the Brillouin function. *J. Phys. A: Math. Gen.* **19**, 1179–1187.

Szego, G. (1939). *Orthogonal Polynomials*. Rhode Island, Providence: American Mathematical Society.

Thole, B.T., Van Der Laan, G. & Sawatzky, G.A. (1985). Strong magnetic dichroïsm predicted in the $M_{4,5}$ X-ray absorption spectra of magnetic rare-earth materials. *Phys. Rev. Lett.* **55**, 2086–2088.

Turck-Chieze, S., Loisel, G., Gilles, D., Piau, L., Blancard, C., Blenski, T., Busquet, M., Cosse, P., Delahaye, F., Faussurier, G., Gilleron, F., Guzik, J., Harris, J., Kilcrease, D.P., Magee Jr., N.H., Pain, J.-C., Porcherot, Q., Poirier, M., Zeippen, C., Bastiani-Ceccotti, S., Reverdin, C., Silvert, V. & Thais, F. (2011). Radiative properties of stellar plasmas and open challenges. *Astrophys. Space Sci.* **336**, 103–109.

Voigt, W. (1912). Sitzber. K. B. Akad. Wiss. München, p. 603.

https://doi.org/10.1017/S0263034615000257 Published online by Cambridge University Press